Available online at www.sciencedirect.com

ScienceDirect

Procedia Structural Integrity 17 (2019) 206–213

Structural Integrity Procedia

www.elsevier.com/locate/procedia

ICSI 2019 The 3rd International Conference on Structural Integrity

Effect of Pretreatment on Interface Stability and Morphology of Ni/Al Hybrid Foams by *in situ* Microcantilever Fracture Experiment

Jutta Luksch[a,b] , Anne Jung[a], Christoph Pauly[c], Christian Motz[b], Frank Mücklich[c], Florian Schaefer[b,*]

[a]*Saarland University, Applied Mechanics, Campus A4.2, 66123 Saarbruecken, Germany*
[b]*Saarland University, Materials Science and Methods, Campus D2.3, 66123 Saarbruecken, Germany*
[c]*Saarland University, Chair of Functional Materials, Campus D3.3, 66123 Saarbruecken, Germany*

Abstract

Ni/Al hybrid foams are a new class of innovative cellular composite materials consisting of open-cell aluminium (Al) foams electrochemically coated with nanocrystalline nickel (Ni). They may be used for lightweight construction elements or as crash energy absorbers. The Ni coating strengthens the Al foam achieving an up to ten times higher energy absorption capacities compared to the Al basis foam. Cellular materials such as foams provide a strong structure-property relationship as the macroscopic material properties strongly depend on the strut geometry and the material properties of the individual struts. The interface stability between the coating and the substrate foam is the dominant contribution in the strengthening mechanism of Ni/Al hybrid foams. Hence, micromechanical characterization is an important task for the design of components made of Ni/Al hybrid foams. A strong interface corresponds to a shear-stiff connection between substrate foam and coating, whereas a soft interface allows sliding between the two phases and hence reduces the buckling stiffness of individual foam struts resulting in lower strength and energy absorption capacity of the macroscopic foam. An increased critical energy release rate for interface cracking was revealed by *in situ* microcantilever bending tests prepared by focused ion beam (FIB) during bending tests in the scanning electron microscope (SEM) after the chemical pretreatment of the base foam.

Peer-review under responsibility of the ICSI 2019 organizers.

* Corresponding author. Tel.: +49-681-302-5172; fax: +49-681-302-5015.
E-mail address: f.schaefer@matsci.uni-sb.de

2452-3216
Peer-review under responsibility of the ICSI 2019 organizers.
10.1016/j.prostr.2019.08.028

Keywords: interface stability; hybrid foam; microbeam bending; mircocantilever; FIB tomography

1. Introduction

Metallic foams are bio-inspired materials. Similar to the trabecular architecture of the cancellous bone (build of substantia spongiosa ossium) these cellular, hierarchically structured materials offer an outstanding capacity for energy absorption e.g. in crash applications (Garcia-Morena (2016), Schaedler and Carter (2016)), whereby foams belong to the class of lightweight materials although they offer a high static strength. Hybrid foams are a special class of multimaterial composite foams e.g. copper/aluminium (Cu/Al) hybrid foams (Sun et al. (2015)) and Ni/polyurethane hybrid foams (Jung and Diebels (2016)). Ni/Al hybrid foams consist of an Al basis foam coated with a nanocrystalline or ultra-fine grained layer of Ni (Bouwhuis et al. (2009), Jung et al. (2011)) and offer improved mechanical properties compared to conventional non-hybrid foams with the same density.

The performance of cellular solids can be traced back to their structure on three hierarchical scales (Degischer (2002)), the macro-, meso- and microscale, the so-called MMM-principle (Fig. 1). The macroscale considers the complete foam, the mesoscale performance is governed by pore deformation and on the microscale the deformation and failure of single struts characterizes the mechanical behaviour. On the scale of the struts the load-bearing capacity depends strongly on their microstructure (Mukherjee et al. (2017)) and the decohesion behaviour of the coating. As a consequence of this hierarchical concept, the global macroscopic material behaviour is dominated by micromechanical properties of the struts and the pore structure of the foams. Especially, the mechanical properties of the strut material influence the energy absorption efficiency significantly more than the geometry of the strut or the pores (Jung and Diebels (2017), Kader et al. (2016), Kaya et al. (2016)). Therefore, variations at the mesoscale and microscale lead to strong variations in the overall behaviour of the foams and further development of such microheterogeneous materials with their hierarchical structure needs an analysis based on the concept of scale separation.

A lot of research has been done during the last decades on the mesoscale, but only little work concentrates on the microscale although simulations need structural and mechanical information about the strut material. However, measurements on the microscale are difficult and a very challenging task. Such experiments have to be carried out at well-chosen locations and need very sensitive and well-calibrated load and displacement measurements.

The rapid development of testing rigs for *ex* and *in situ* micro- and nanomechanical testing in combination with the availability of focused ion beam (FIB) systems for micromanufacturing triggered the mechanical testing on the micro-

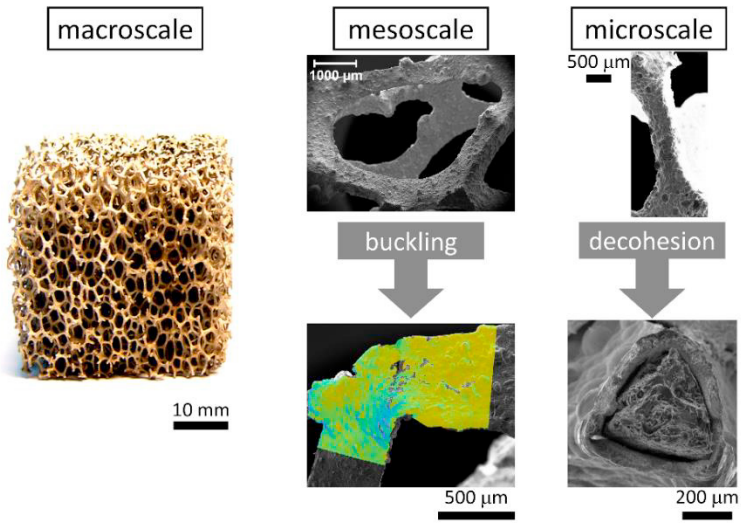

Fig. 1. Ni/Al hybrid foam on macro-, meso- and microscale and typical failure mechanisms. On the mesoscale buckling of individual strut leads to the collapse of pores, whereby the buckling is triggered by decohesion of the Ni coating on the microscale

and nanoscale. These experiments revealed size effects during plastic deformation of metals during the last two decades as shown inter alia by Eisenhut et al. (2017), Motz et al. (2005), Volkert and Lilleodden (2006) and Nix et al. (2007). Besides the nowadays very common micropillar testing, as performed e.g. by Uchic et al (2004) and reviewed e.g. by Kiener et al. (2009), microcantilever bending tests proved to be a powerful tool for the investigation of local mechanical properties on the nanoscale such as strain induced grain growth in nanocrystalline materials (Kapp et al. 2017), fracture toughness of small specimens (Ast et al. (2016), Dehm et al. (2018), Pippan et al. (2017) and Gruenewald et al. (2018)) and even the fracture toughness of individual grain boundaries as shown by Kupka and Lilleoden (2012) and Kupka et al. (2014).

In many applications the interface stability and the deformation resistance near and over these internal interfaces govern the material properties. The well-known Hall-Petch-relation (Hall (1951)) is just one out of many examples of how important the presence and the resistance against slip transfer of grain boundaries is. As the typical interfaces in materials on the microscale grain boundaries influence strongly the deformation behaviour of metals on the macroscale.

During compressive deformation of foams, bending and buckling of the struts, under the fixed boundary conditions of the pore network, is the base failure mechanism (Fig. 1). Bending and buckling are affected strongly by the connection and shear-stiffness at the interface between the Ni coating and the Al basis foam that vanishes in the case of decohesion.

In the present study, *in situ* microcantilever bending and fracture experiments were employed to investigate the interface stability between the Ni coating and Al substrate foam. The critical deformation energy dissipation for interface crack initiation and interface failure was measured by quasi-static crack growth. The interface damage behaviour was linked to the interface morphology by 3D FIB tomography and reconstruction. A chemical pretreatment of the substrate Al foam was shown to improve the fracture toughness of the interface.

2. Materials and Methods

2.1. Ni/Al hybrid foams

The $AlSi_7Mg_{0.3}$ Al alloy foams of a pore size of 10 pores per inch (ppi) was manufactured by CellTec Materials GmbH, Dresden, Germany, by investment casting. A coating with a hard facing Ni layer of about 50 µm produced by electrodeposition (Jung et al. (2011), Jung et al. (2016)) enhances the mechanical properties. A commercial nickelsulfamate electrolyte with 110 g/l Ni, Enthone GmbH, Langenfeld, Germany, was used at a temperature of 50 °C with a pH of 3.8 for the plating. For better adhesion of the coating on the Al a pretreatment of pickling and electroless plating of zinc (Zn) was conducted with multiple repeats. The plating protects the Al foam from dissolution in the acid electrolyte and enhances the adhesion of the coating. To study if the pretreatment, as a time-consuming additional step

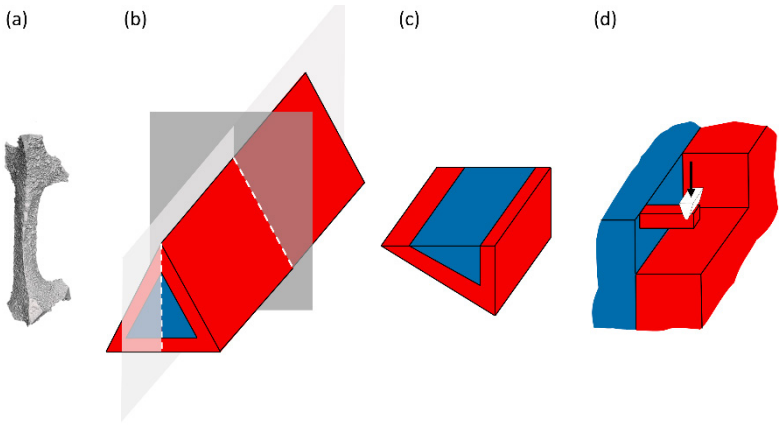

Fig. 2: (a) shape of a foam strut, (b) preparation planes by grinding and polishing of a strut, (c) strut segment for FIB preparation, (d) prepared microcantilever with tip

in the production of the hybrid foam, is necessary, two different states of the hybrid foam were investigated: one pretreated foam and one untreated foam.

As a first preparation step, a volume of about 1 x 1 x 1 cm^3 was carefully extracted with a small side cutter out of a macroscopic hybrid foam specimen of each state. The subsequent preparation was performed by grinding (600, 1200 and 2400 grit) and diamond polishing (6, 3 and 1 µm). The specimen was embedded in a dissolvable resin Technovit® 5075, Kunzer GmbH, Hanau, Germany, to minimize the force during mechanical preparation. After the preparation the resin was removed using acetone. One strut was sectioned along its axis in order to ensure that the interface is perpendicular to the prepared surface. Another cross-section perpendicular to the first one forms a defined second edge (Fig. 2 (b)) for the FIB preparation with a Helios NanoLab 600 from FEI Company, Hillsboro, USA.

2.2. Tomography

The FIB tomography was performed on a well-chosen and representative area of 10 x 10 $µm^2$ with a prior platinum deposition to protect the analyzed volume from gallium implantation and artefacts like curtaining. For alignment during the automatic tomography by slice by slice sectioning a cross fiducial was milled. A U-shaped free cut prevents shading during image collection by SEM. The tomography was conducted with a slice thickness of 30 nm. The secondary electron images were collected with an acceleration voltage of 5 keV.

The software Amira from FEI Company, Hillsboro, USA, was used for the 3D reconstruction. An alignment of the images was conducted before the segmentation step, primarily by manual rearrangement. The characteristic volume, surface, shape and number of particles of the involved materials was analyzed using the software MAVI from Fraunhofer Institute for Industrial Mathematics (ITWM), Kaiserslautern, Germany.

2.3. Evaluation of the critical energy dissipation

Microcantilevers prepared with the FIB were cut in the Ni coating and thereafter the interface was positioned at the suspension of the cantilever since here the load was expected to reach its maximum according to FEM simulations. An ion beam current of 21 nA and 6.5 nA was used for the rough cutting followed by a polishing with 0.92 nA and 0.48 nA to reduce gallium implantation and to ensure a good quality of the specimen surface. A 1.5 µm notch was cut with an ion beam current of 48 pA to ensure a small notch radius of less than 100 nm. This small notch localizes the stress concentration to the interface during bending.

The *in situ* bending tests were conducted with a nanoindenter UNAT2 from Asmec/ZwickRoell, Dresden, Germany, in a Zeiss Sigma, Oberkochen, Germany, SEM. The wedge-shaped tungsten carbide tip, positioned at a distance of 30 µm from the interface (cantilever arm length), bent the cantilevers stepwise with unloading segments used for a compliance measurement. The wedge-shaped tip was given a radius of 5 µm to promote smooth unrolling on the cantilever's surface. Every 0.4 µm an unloading segment of 0.2 µm was performed and used to calculate the compliance offline. A reduction of the measured force indicates a crack growth.

A displacement-controlled finite element method (FEM) co-simulation with Abaqus® from Dassault Systémes, Vélizy-Villacoublay, France, enables a calculation of the crack length from the measured compliance. The cantilever was simulated with identical geometry and the material parameters were taken from literature. The friction coefficient between the rigid wedge and elastic cantilever was set to 0.4 during a default hard contact. The crack was represented by unconnected nodes of the hexahedral quadratic elements (seem crack in C3D20 elements). The Al part of the specimen geometry was fixed.

The compliance proved to be linearly dependent on the crack length over a wide range of crack lengths from 10 % up to 90% of the cantilever thickness regarding the notch depth of about 20 % of the cantilever thickness. Hence, for the further evaluation the crack length can be deducted from the measured experimental compliance.

The area below the force-displacement curve corresponds to the dissipated energy during deformation and can be split to an elastic and plastic part by an extrapolation of the unloading segments to zero load. Finally, the measured dissipated energy is plotted versus the crack length. The energy evolution during crack growth is a measure for stable and unstable crack growth. A scheme of this evaluation is shown in Fig. 3.

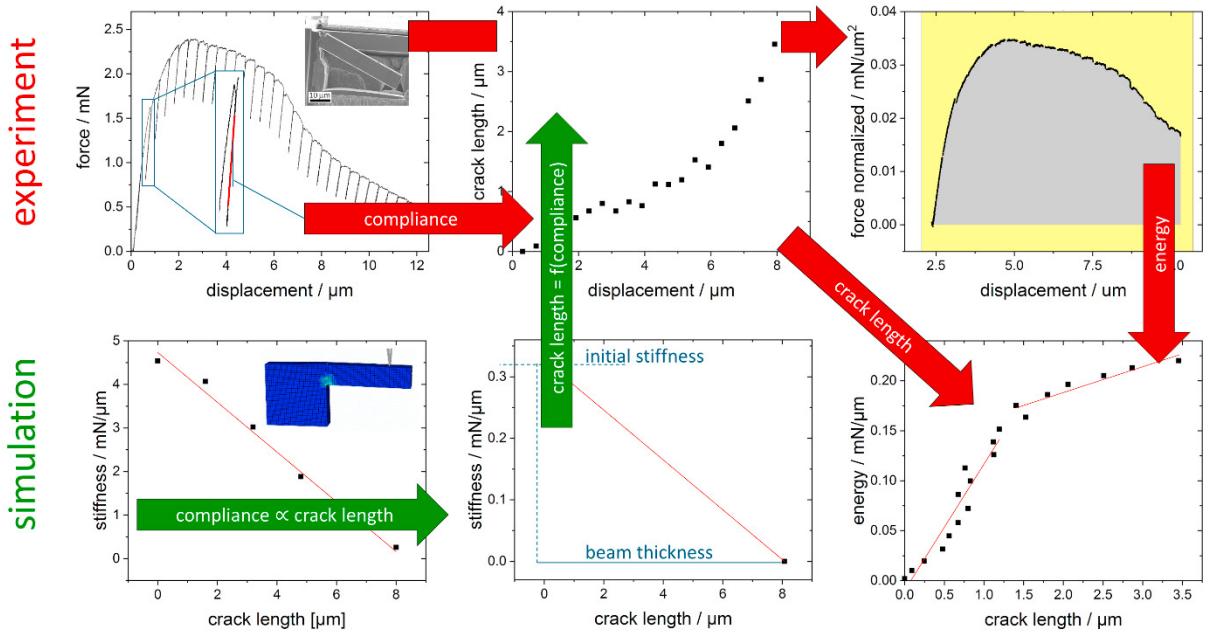

Fig. 3. Schematic representation of data evaluation: the crack length is calculated from the experimentally measured compliance after FEM co-simulation of the cantilever stiffness evolution of the increasing crack length (reduction of the ligament) and the crack length is opposed to the energy absorption during bending deformation.

3. Results and Discussion

Fig. 4 shows the two 3D reconstructed volumes of 8 x 8 x 8 µm^3 from the FIB tomography for the pretreated (pt) and untreated (ut) specimen. The pretreated specimen has a jagged and fragmented interface with pore clusters with a size in the order of a few micrometers. The pore clusters of the pretreated specimen are much larger than those of the untreated specimen. The interface of the untreated specimen also shows a much smoother morphology. Thus the interface between the Al alloy and Ni coating is larger for the pretreated than for the untreated specimen. The tomography also revealed a silicon (Si) precipitate from the Al cast alloy inside the reconstructed volume as well as on the interface. The interfaces between the precipitate and the Ni and Al alloy phase are smooth as well. Therefore, a reduced cohesion of the coating on the Al basis foam was expected for the pretreated case because it shows significantly more pores, although the morphology resembles a snap-like connection with many undercuts.

As seen in the SEM images (Fig. 5 (c)) the cantilever from the untreated specimen breaks more or less brittle along the interface. In contrast, the interface in the cantilever from the pretreated specimen breaks along the pore clusters, predominantly on the Al side of the interface. Al is ductile and the weakest points of the interface are, as revealed by the tomography, the pore clusters on the Al side of the interface. During testing the cantilever from the pretreated specimen the deformation started in the Al alloy, consecutively crack growth occurred by extending the pores and afterwards by cracking along the pores via pore coalescence. The *in situ* observations indicates that the failure of the interface of the pretreated specimen has an ineligible ductile component whereas the interface of the untreated specimen is prone to brittle failure with only minor visible plastic deformation in the interface region.

For the two tested microcantilevers the rectangular cross-sectional area is not equal. Therefore, the force was normalized by the cross-sectional area for the further data analysis. The normalized force-displacement curve for the untreated specimen (Fig. 6 (a)) shows a significant drop in the load past the load maximum. The force-displacement curve for the pretreated specimen shows no spontaneous force drop. The force decreases continuously after reaching the force maximum. From the unloading segments in the normalized force-displacement data, the compliance was calculated and the crack length was derived from the experimental compliance of the FEM experiments.

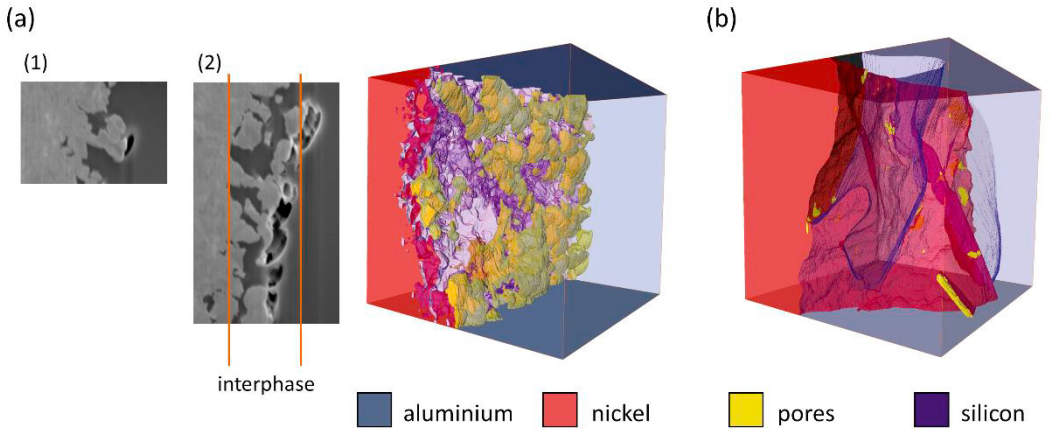

Fig. 4. Comparison of the morphology of the interface of a (a) pretreated specimen with (1) SEM image of an undercut and (2) SEM image of the interface and (b) untreated specimen from FIB tomography and 3D reconstruction.

For each unloading segment, the total elastic and plastic area under the normalized force-displacement curve was evaluate and plotted versus the crack length in the absorbed energy-crack length diagram (Fig. 6 (b)). The microcantilever from the untreated specimen shows a steep increase of the energy dissipation with crack length indicating brittle material behavior. After reaching a crack length of 0.2 µm the gradient of the curve is much lower. This decreasing energy dissipation was linked with accelerated crack growth with the beginning of a less stable crack growth behavior.

The cantilever from the pretreated specimen, on the contrary, shows a smaller increase of the dissipated energy during the initial crack growth in the energy-crack length curve. The smaller increase of the dissipated energy indicates minor crack growth resistance. After reaching a critical crack length of 1.25 µm, the gradient decreases. Table 1 gives an overview of the data from the analysis of the microcantilevers. A steep increase in the initial energy-crack length curve is typical for brittle failure, whereas unstable crack growth would be characterized by a constant dissipated energy with further crack propagation. In contrast, crack growth accompanied by an increase of the dissipated energy is known from ductile behavior such as pore extension and coalescence. Therefore, the change in the gradient of the dissipated energy-crack length curve can be associated with a critical energy dissipation that characterizes the interface

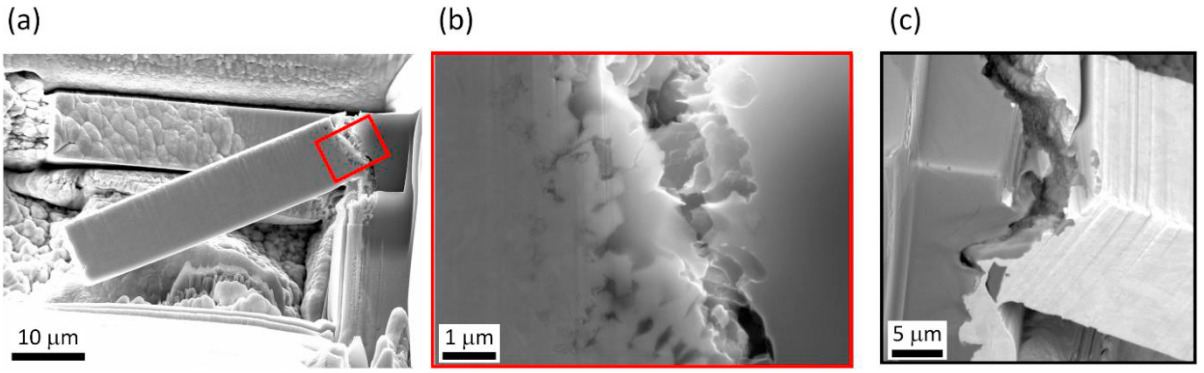

Fig. 5. (a) microcantilever of the pretreated specimen after the experiment. (b) detail from (a) that shows that the crack follows the pores after they connected to each other. (c) untreated microcantilever with crack along the interface post mortem. The Ni surface from the former interface is clearly visible on the crack surface.

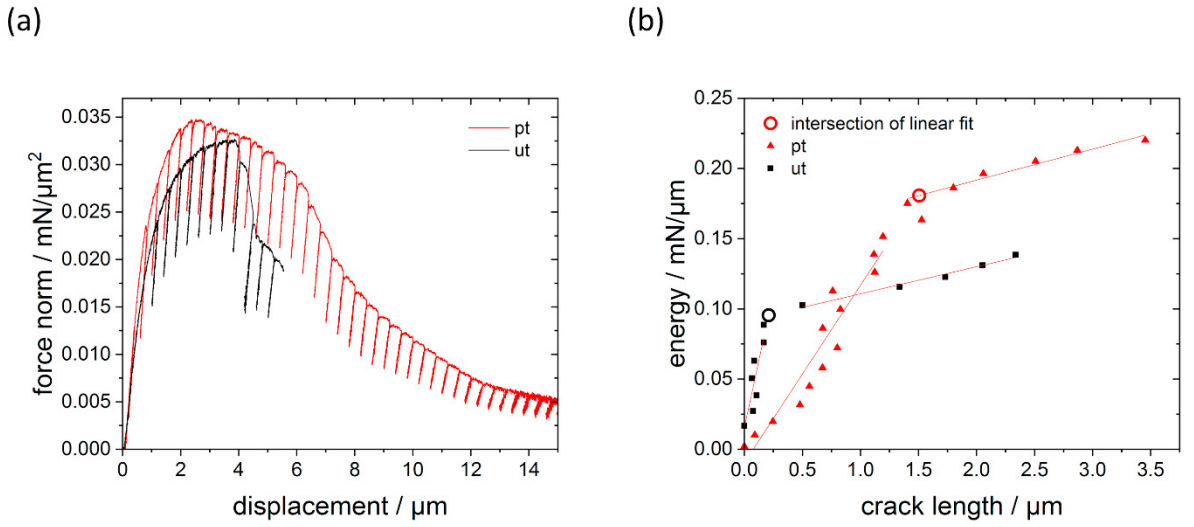

Fig. 6. (a) normalized force-displacement curve with unloading segments for microcantilever bending from pretreated (pt) and untreated (ut) specimen. (b) absorbed energy vs. crack length curve of both data sets with fit lines.

fracture toughness comparable to the J-integral in standard fracture toughness evaluation. Hence, we conclude that the untreated specimen fails by more brittle interface cracking, whereas the pretreated interface fails by ductile failure mechanisms with a higher fracture toughness compared to the untreated case.

Table 1. Overview of cantilever geometry and test results: cantilever thickness t, cantilever width w, cross section area A, maximum force F_{max}, normalized maximum force $F_{max,\,norm}$, critical energy E_{crit}

specimen	t / µm	w / µm	A / µm²	F_{max} / mN	$F_{max,\,norm}$ / mN/µm²	E_{crit} / mN/µm
pt	9.57	7.19	68.88	2.39	0.0348	0.1807
ut	7.29	7.60	55.40	1.81	0.0327	0.0954

4. Conclusion

The *in situ* observations and data evaluation from the bending tests in combination with the FIB tomography demonstrated that the morphology of the interface has a strong impact on the decohesion resistance of the interface in hybrid foams. The pretreatment of the Al alloy foam produces a jagged and fragmented surface, which leaves pore networks due to the coating process by electrodepostion. The structure might be described as snap fastened and has a tight fit connection. The adhesion of the coating to the Al alloy is much more stable for the pretreated foam because the specimen from the pretreated foam does fail ductilely at the interface with a higher critical energy. The interface of the untreated specimen has a smooth morphology and failure occurs as brittle interface cracking. The pretreatment leads to a more stable cohesion. The pushbutton-like structure of the interface after a pretreatment has a stabilizing effect due to the shape and larger interface area between Al cast alloy and Ni. The pore clusters on the Al side of the interface are the weak parts of the structure. To improve the pretreatment a goal would be to minimize the pore clusters.

In this context it might not be ideal, to consider the layer between Ni and Al as interface as the pretreated specimen rather has an interphase consisting of a two-phase-volume with pores instead of a smooth interface as found in the untreated specimen. The pores are encompassed mainly by the Al phase (Fig. 4 (a)). In contrast, the untreated specimen has a sharp interface between the Al foam and the Ni coating.

The method of *in situ* microcantilever fracture experiments in combination with FIB tomography of the interface, invented and successfully tested for the issue of quantifying the interface stability between a coating and a base foam

on the microscale allows to further improve the interface morphology by a varied chemical pretreatment and therefore a further improvement of the energy absorption capacity of hybrid foams on the macroscale in the future.

Acknowledgements

We thank Michael Fries from Saarland University for manufacturing the specimen material. We also are indebted to Michael Engstler from Saarland University his assistance during the 3D reconstruction. We thank Jonas Rauber for effort during proof-reading.

References

Ast, J., Merle, B., Durst, K., Göken, M., 2016. Fracture toughness evaluation of NiAl single crystals by microcantilevers—a new continuous J-integral method. Journal of Materials Research 31(23), 3786-3794.

Bouwhuis, B. A., McCrea, J. L., Palumbo, G., Hibbard, G. D., 2009. Mechanical properties of hybrid nanocrystalline metal foams. Acta Materialia 57(14), 4046-4053.

Degischer, H.-P., Kriszt, B., 2002. Handbook of Cellular Metals, Wiley-VCH Weinheim.

Dehm, G., Jaya, B. N., Raghavan, R., Kirchlechner, C., 2018. Overview on micro-and nanomechanical testing: New insights in interface plasticity and fracture at small length scales. Acta Materialia 142, 248-282.

Eisenhut, L., Schaefer, F., Gruenewald, P., Weiter, L., Marx, M., Motz, C., 2017. Effect of a dislocation pile-up at the neutral axis on trans-crystalline crack growth for micro-bending fatigue. International Journal of Fatigue 94, 131-139.

García-Moreno, F., 2016. Commercial applications of metal foams: Their properties and production. Materials 9(2), 85.

Gruenewald, P., Schaefer, F., Thielen, M., Marx, M., Motz, C., 2018. Small scale fracture mechanics of ductile materials: Advantage of fatigue precracks and comparison of J-integral evaluations. Materialia 4, 104-108.

Hall, E. O., 1951. The deformation and ageing of mild steel: III discussion of results. Proceedings of the Physical Society. Section B 64(9), 747-753.

Jung, A., Chen, Z., Schmauch, J., Motz, C., Diebels, S., 2016. Micromechanical characterisation of Ni/Al hybrid foams by nano-and microindentation coupled with EBSD. Acta Materialia 102, 38-48.

Jung, A., Diebels, S., 2016. Synthesis and mechanical properties of novel Ni/PU hybrid foams: a new economic composite material for energy absorbers. Advanced Engineering Materials 18(4), 532-541.

Jung, A., Diebels, S., 2017. Microstructural characterisation and experimental determination of a multiaxial yield surface for open-cell aluminium foams. Materials & Design 131, 252-264.

Jung, A., Natter, H., Diebels, S., Lach, E., Hempelmann, R., 2011. Nanonickel coated aluminum foam for enhanced impact energy absorption. Advanced Engineering Materials 13(1-2), 23-28.

Kader, M. A., Islam, M. A., Saadatfar, M., Hazell, P. J., Brown, A. D., Ahmed, S., Escobedo, J. P., 2017. Macro and micro collapse mechanisms of closed-cell aluminium foams during quasi-static compression. Materials & Design 118, 11-21.

Kapp, M. W., Kremmer, T., Motz, C., Yang, B., Pippan, R., 2017. Structural instabilities during cyclic loading of ultrafine-grained copper studied with micro bending experiments. Acta Materialia 125, 351-358.

Kaya, A. C., Zaslansky, P., Nikolaus, A., Fleck, C., 2016. Tensile failure observations in sintered steel foam struts revealed by sub-micron contrast-enhanced microtomography. Materials & Design 105, 190-200.

Kiener, D., Motz, C., Dehm, G., 2009. Micro-compression testing: A critical discussion of experimental constraints. Materials Science and Engineering A505(1-2), 79-87.

Kupka, D., Huber, N., Lilleodden, E. T., 2014. A combined experimental-numerical approach for elasto-plastic fracture of individual grain boundaries. Journal of the Mechanics and Physics of Solids 64, 455-467.

Kupka, D., Lilleodden, E. T., 2012. Mechanical testing of solid–solid interfaces at the microscale. Experimental mechanics 52(6), 649-658.

Motz, C., Schöberl, T., Pippan, R., 2005. Mechanical properties of micro-sized copper bending beams machined by the focused ion beam technique. Acta Materialia 53(15), 4269-4279.

Mukherjee, M., García-Moreno, F., Jiménez, C., Rack, A., Banhart, J., 2017. Microporosity in aluminium foams. Acta Materialia 131, 156-168.

Nix, W. D., Greer, J. R., Feng, G., Lilleodden, E. T., 2007. Deformation at the nanometer and micrometer length scales: Effects of strain gradients and dislocation starvation. Thin Solid Films 515(6), 3152-3157.

Pippan, R., Pfeifenberger, M., Wurster, S., Kapp, M., Hartl, S., Kiener, D., 2017. Fracture mechanics of microsamples.

Schaedler, T. A., Carter, W. B., 2016. Architected cellular materials. Annual Review of Materials Research 46, 187-210.

Sun, Y., Burgueño, R., Wang, W., Lee, I., 2015. Modeling and simulation of the quasi-static compressive behavior of Al/Cu hybrid open-cell foams. International Journal of Solids and Structures 54, 135-146.

Uchic, M. D., Dimiduk, D. M., Florando, J. N., Nix, W. D., 2004. Sample dimensions influence strength and crystal plasticity. Science 305, 986–989.

Volkert, C. A., Lilleodden, E. T., 2006. Size effects in the deformation of sub-micron Au columns. Philosophical Magazine 86(33-35), 5567-5579.